PHYSICAL REVIEW B **77**, 195422 (2008)

Solid-state dewetting-mediated aggregation of nanoparticles

J. S. Palmer, P. Swaminathan, S. Babar,* and J. H. Weaver
Department of Materials Science and Engineering, University of Illinois at Urbana-Champaign, Urbana, Illinois 61801, USA
(Received 7 February 2008; published 15 May 2008)

The deposition of Au onto thin Xe films at a low temperature leads to cluster formation. The subsequent Xe sublimation results in cluster aggregation and delivery to the substrate in a process known as buffer-layer-assisted growth. Previously, this process was described in terms of a diffusion-limited cluster-cluster aggregation process during layer-by-layer desorption of the buffer. Instead, significant diffusion, restructuring, and dewetting of the Xe occur prior to desorption, and this leads to cluster aggregation. Cluster motion and aggregation are driven by capillary forces as the dewetting film retreats and sublimes. Kinetic Monte Carlo simulations reproduce the experimentally observed particle shapes and size distributions, and they provide additional insight into the interaction of the particles with the dewetting front. The presence of nanoscale particles on the film inhibits dewetting and significantly alters the shape of the front.

DOI: 10.1103/PhysRevB.77.195422 PACS number(s): 68.65.−k, 36.40.Sx, 61.46.Df, 68.08.Bc

I. INTRODUCTION

Capillary forces at the interfaces between particles, fluids, and solid substrates lead to the self-assembly of structures during liquid film evaporation.[1] Coffee or salt rings left after evaporation provide a glimpse of the intriguing nonequilibrium interactions of particles with volatile films. Fluid flow, which can result from temperature variations[2] or flow to a pinned contact point,[3,4] plays a critical role in the patterns left on the surface. Here, we introduce a related process that involves nanoparticle assembly during dewetting and sublimation of a *solid* thin film, wherein bulk diffusion is limited.

In a technique known as buffer-layer-assisted growth (BLAG), atoms evaporated onto condensed inert gas films such as Xe form clusters that can be delivered to a substrate of choice by subliming the buffer.[5,6] The inert buffer not only allows for the formation of clusters, but its removal plays a key role in the assembly of those clusters. The images in Fig. 1 provide examples of clusters produced by the BLAG process on 4 and 40 monolayer (ML) Xe films condensed onto amorphous carbon (*a*-C). During buffer removal, the clusters move and aggregate. For thin buffers, the resulting particles are small and compact. As the thickness increases, they become much larger and ramified, and the average sizes and densities of the clusters have a power law dependence on the buffer thickness.

This aggregation process was previously modeled as particle diffusion on the inert gas surface during layer-by-layer sublimation of the film.[7,8] We present experimental evidence that a significant restructuring of the buffer takes place and that, as for liquids, the physics underlying cluster aggregation involves capillary forces as the film dewets the substrate. Moreover, the particles influence the dynamics of the movement of the dewetting front by inhibiting Xe surface diffusion. Because multilayers of condensed gases do not, in general, completely wet solid substrates,[9] this nanoparticle assembly process occurs in a variety of systems wherein particles are grown on thin volatile films condensed on different substrates. Examples include magnetic[10] or II-VI semiconductor[11] particles, carbon dioxide[12] or ice[13] films, and semiconductor[6] or metallic[14] substrates.

II. EXPERIMENT

The samples were grown in an ultrahigh vacuum chamber with a typical base pressure below 1×10^{-10} Torr. The substrates were 20–30-nm-thick *a*-C foils supported on copper grids that were degassed *in vacuo* for ~24 h at 125–150 °C. The samples were mounted on copper holders attached to the coldhead of a closed-cycle He refrigerator, and Xe films were condensed at 20 K from a background pressure of a high purity gas. Film thicknesses are reported in ML, where 1 ML of Xe(111) results from a 3.5 s exposure at 1×10^{-6} Torr and corresponds to 6×10^{14} atoms cm^{-2}. Au was thermally evaporated onto the film at a rate of ~1 Å per minute, and average thicknesses were determined by using a calibrated thickness monitor. The samples were warmed by radiation and conduction through the coldhead when the helium refrigeration was turned off. During the thermal treatment experiments, the samples were warmed at ~1.5 K min^{-1} until reaching the specified temperature and then were immediately cooled at ~4.5 K min^{-1} to 20 K. Sample characterization was done at room temperature with a Philips CM12 120-kV transmission electron microscope (TEM).

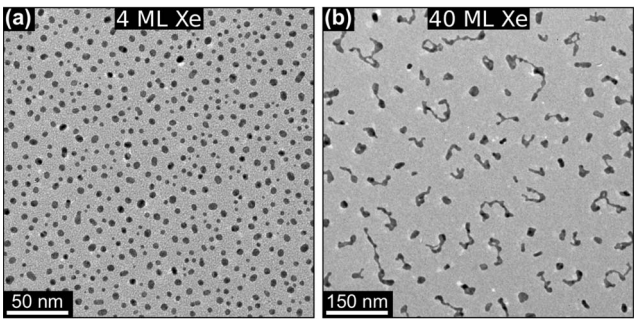

FIG. 1. Clusters formed by depositing 5 Å of Au on 4 and 40 ML Xe films condensed at 20 K on *a*-C. Images were obtained after heating to sublime the Xe. For thin Xe buffers, the clusters are small and compact. Thicker buffers lead to the formation of larger ramified aggregates.

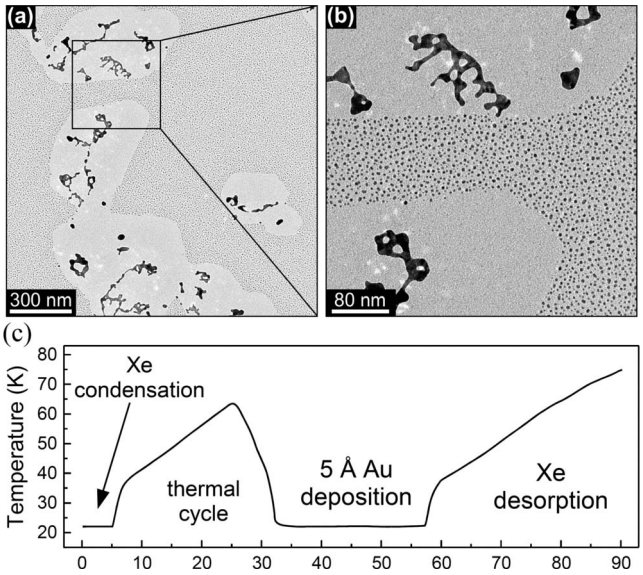

FIG. 2. (a) Low and (b) higher magnification TEM micrographs of clusters formed on a dewet Xe buffer. The images show a bimodal distribution, indicating that the Xe film dewet to expose *a*-C and form islands. Larger clusters were formed on these islands, while the high-density clusters directly formed on the *a*-C. The buffer was prepared by condensing 40 ML of Xe onto *a*-C at 20 K. As depicted in (c), the sample was warmed to 64 K and then cooled to 20 K prior to a 5 Å Au deposition and further dewetting during warm up to room temperature.

III. RESULTS AND DISCUSSION

A. Structural changes prior to desorption

Recent studies demonstrated that Xe condensed at 34 K initially results in multilayer islands on *a*-C, which indicate a significant Xe diffusion.[15] Continued Xe deposition leads to island coalescence and the formation of kinetically trapped layers. As for unstable thin metal and ceramic films, heating allows voids to form at defects or grain boundary triple points through grain boundary grooving.[16,17] Capillary forces account for void spreading and film breakup.

Dewetting of thin Xe films can be observed by thermally cycling the Xe film and then depositing Au to decorate the exposed (dewet) regions of the substrate. The size and density of the formed Au clusters can be used to determine the local thickness of the Xe film after heat treating. Figures 2(a) and 2(b) demonstrate such dewetting for a film that was initially 40 ML thick. As depicted in Fig. 2(c), the buffer was condensed at 20 K and the sample was warmed to 64 K, cooled back to 20 K for the Au deposition, and then warmed to room temperature. The regions that had dewet prior to the Au deposition are clearly evident in Fig. 2(a) from the high density of small clusters covering 70% of the surface. These clusters are consistent with Au deposition directly onto *a*-C; they are shown in the higher resolution image in Fig. 2(b). Cluster sizes in the low-density regions indicate that the Xe islands on which the Au was deposited had thickened during dewetting and had an average thickness greater than 100 ML. The bimodal distributions indicate significant film restructuring at temperatures far below the equilibrium melting temperature of 161 K and prior to desorption.

B. Dewetting and cluster aggregation

To understand how particles interact with the buffer during the dewetting that accompanies warmup, we developed one technique for following dewetting and another for probing the cluster aggregation process, as depicted in Fig. 3. The samples were prepared by depositing 5 Å of Au at 20 K on 40 ML Xe films (top center), heated to 65 K to allow partial Xe dewetting, and then cooled to 20 K.

Figure 3(a) was obtained after such a sample was capped with water (amorphous ice) and warmed to ambient temperature. The water was deposited by back filling the chamber from a source purified by a series of freeze, pump, and thaw cycles. The water cap prevented further Xe dewetting, fixing the locations of the particles as Xe escaped through the cap.[18] The low-density regions reveal particles with sizes and densities consistent with Fig. 1(b). The small-cluster, high-density regions reflect the initial state of clusters that had formed on the buffer. They were immobilized by Xe that diffused from the dewet areas and then by the ice cap.

The sample in Fig. 3(b) was prepared as in Fig. 3(a) except that additional Au was deposited without the ice cap. The additional Au highlights the dewet regions, as in Fig. 2, and demonstrates that cluster aggregation was complete in the dewet regions. The region on the left of Fig. 3(b) has large clusters that formed during dewetting and were then supplemented with small ones that have a density and a size consistent with deposition directly onto *a*-C at 20 K. Elsewhere, there are large ramified clusters that formed from a combination of the two Au depositions as dewetting progressed and the film sublimed.

Figure 3(c) was obtained after an ice cap was condensed on a sample similar to that in Fig. 3(b) to show both the location of the dewet regions and the clusters, to confirm the interpretations of Figs. 3(a) and 3(b). The clusters in the dewet region are like those in Fig. 3(b) because their formation was complete before H_2O condensation. In the regions where Xe remained, the cap prevented the aggregation of the small clusters, as in Fig. 3(a).

The intermediate-sized clusters in Figs. 3(a) and 3(c) show that cluster aggregation occurs along the dewetting front. Particles on the dewet side of the front have completed their aggregation, while those on the film side remain in their initial state. These results indicate that the clusters do not diffuse on the buffer, but aggregation occurs as particles move with the dewetting front. Clearly, a new model that takes Xe dewetting and cluster motion with the front into account is needed to replace the earlier diffusion-limited cluster-cluster aggregation (DLCCA) model.

C. Capillary-force-driven particle motion

The motion of the particles with the dewetting front can be understood in terms of capillary forces, as depicted in the atomistic picture in Fig. 4. Because of the relatively high surface energy of Au compared to Xe, the particles will be coated with a layer of Xe. The gain in free energy follows

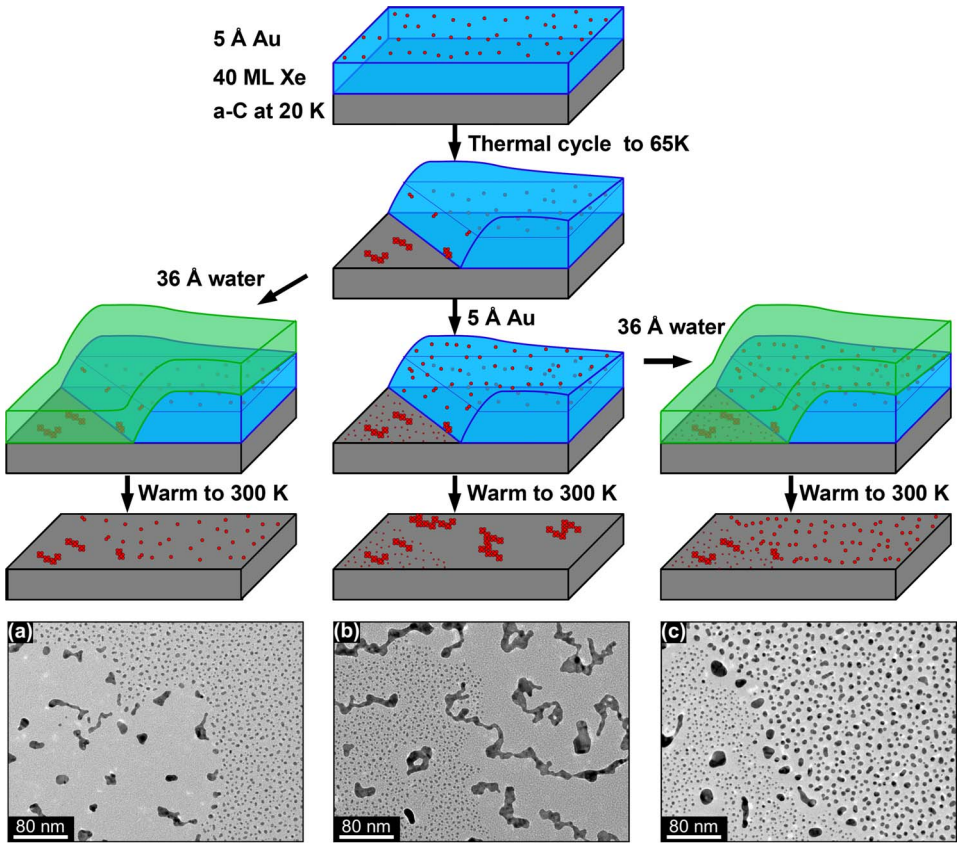

FIG. 3. (Color online) Investigations into the effect of warming a Xe film decorated with Au. Clusters were formed by depositing 5 Å of Au on 40 ML of Xe at 20 K, warming to 65 K to facilitate partial dewetting, cooling to 20 K, doing a second deposition, and warming to room temperature. During this cycle, Xe from the dewetting areas up-diffused to thicken the islands and trap the clusters where they had formed. The second deposition consisted of (a) ~36 Å of ice, (b) 5 Å of Au, and (c) 5 Å of Au followed by ~36 Å of ice. The second deposition revealed the extent of dewetting and cluster aggregation after the heat treatment, as indicated in the diagrams.

from the surface energies of Au and Xe and the Au-Xe interfacial energy, namely, $\Delta\gamma=\gamma_{Xe}+\gamma_{XeAu}-\gamma_{Au}$. By using 1.55 J/m^2, 32.5 mJ/m^2, and 1.35 J/m^2 for the Au, Xe, and Au-Xe energies,[19] we obtain $\Delta\gamma=-0.17$ J/m^2. Further energy could be gained by burrowing into the film, which is driven by a capillary force of approximately $F=2\pi\gamma_{Xe}(z-2r)$, where r is the radius of a spherical particle and z $(0\leq z\leq 2r)$ is the distance the particle has burrowed.[20] The resulting pressure is 32.5 MPa for a spherical cluster of $r=2$ nm (typical for 5 Å of Au deposited onto Xe) burrowed halfway into the film. (The surface energy of Xe is used assuming the particle is already coated.) This pressure drives the diffusion of Xe from beneath the clusters and moves them into the solid film. Such sinking has been predicted for small Cu clusters on Xe by using molecular dynamics simulations,[21] inferred from scanning tunneling microscopy measurements,[14] and followed with photoemission.[22] It has also been observed with atomic force microscopy for Co particles on metal films.[20,23]

The capillary force that leads to burrowing also draws the particles with the dewetting front, as depicted in Fig. 4. In Fig. 4(a), the Au clusters are coated with Xe and have been partially buried by burrowing and by Xe transported from the dewet areas. When the dewetting edge reaches a cluster, it begins to uncover it [Fig. 4(b)], but capillary forces keep the cluster moving with the front [Fig. 4(c)]. Such clusters eventually collide to form aggregates [Fig. 4(d)] that can coalesce and shift or rotate to form a better contact with each other and the buffer. The aggregates are left behind as the dewetting front moves around them or they become pinned to the substrate. They come to rest on the substrate when all of the Xe has sublimed.

D. Kinetic Monte Carlo simulation of aggregation

The cluster shapes and size distributions were explained earlier with a DLCCA model.[7,8,24] The obvious question introduced by the evidence of dewetting is whether those shapes and size distributions can be explained by using a model based on motion driven by capillary forces with a dewetting front. To this end, we modified a Monte Carlo model of drying-mediated nanoparticle assembly in liquid films[25] to account for limited cluster mobility. A crucial difference is that we assume that particles do not undergo a

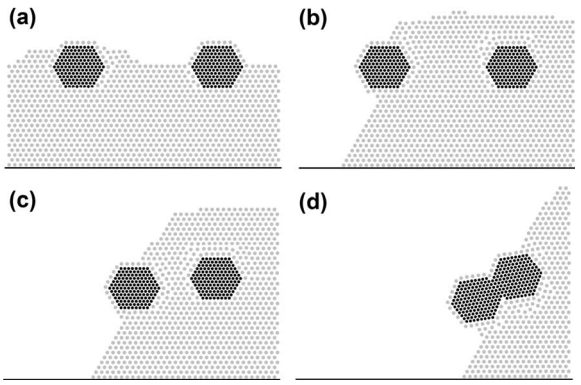

FIG. 4. A cross-sectional atomistic model of capillary forces moving a cluster with a dewetting front, bringing two clusters into contact. Initially the 2 nm radius Au clusters burrow into the 20 ML Xe film. The dewetting film first covers them in (a) and then exposes them in (b). Movement with the dewetting front in (c) leads to cluster aggregation in (d).

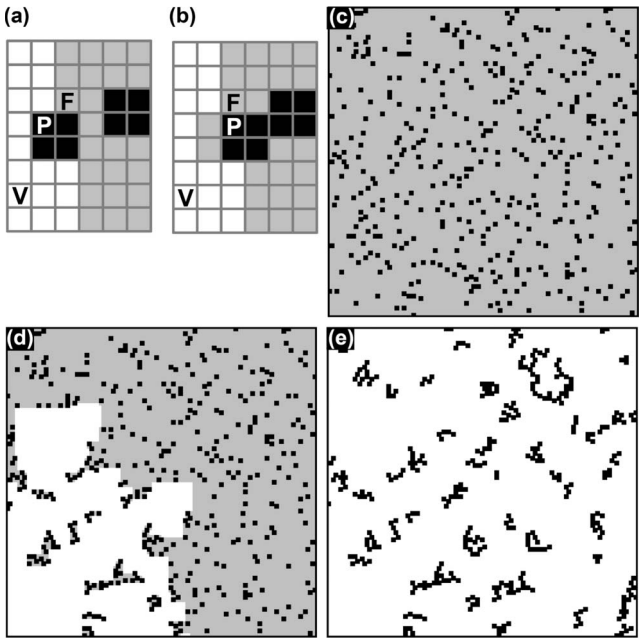

FIG. 5. Cluster assembly modeled on a two-dimensional lattice. Nearest neighbor interactions are used to determine dewetting probabilities and particle (P) motion at the film (F)-vacuum (V) interface. (a) and (b) depict particle motion, and (c), (d), and (e) show initial, intermediate, and final states, respectively, of a kinetic Monte Carlo simulation with $\beta=10^{14}$. Shown is a 128×128 portion of a 512×512 lattice. (d) Particles aggregate at the dewetting edge and are deposited on the substrate.

random walk as they could in a liquid because of the low particle diffusivity on the solid film and substrate. Rather, particle motion is driven by their interaction with the film and vacuum. Moreover, when two particles come in contact, they irreversibly stick and a subsequent motion is concerted.

Our model is a two-dimensional lattice wherein each site contains vacuum (V), film (F), or nanoparticle (P), as shown in Fig. 5. Figure 5(a) provides a top-down view of the model. Site V has undergone dewetting, particle P is on the dewetting front, and the other particle has burrowed into the film away from the dewetting front. The energy of the system is defined by nearest neighbor interactions as follows:

$$H=-\sum_{\langle i,j\rangle}\varepsilon_{ij}|S_iS_j|, \tag{1}$$

where the sum is over all nearest neighbor pairs. $S=-1$ for film, 0 for vacuum, and 1 for particle sites. The interaction is given by

$$\varepsilon_{ij}=\varepsilon_{ff}\delta_{-1S_i}\delta_{-1S_j}+\varepsilon_{pp}\delta_{1S_i}\delta_{1S_j}+\varepsilon_{fp}[\delta_{-1S_i}\delta_{1S_j}+\delta_{1S_i}\delta_{-1S_j}], \tag{2}$$

where ε_{ff}, ε_{fp}, and ε_{pp} are the free energies that correspond to nearest neighbor interactions and δ is the Kronecker delta function.

Initially, lattice sites are randomly chosen to be filled with particles and the remainder are filled with film, as in Fig. 5(c). During each step, a film site is converted to vacuum, which represents dewetting, or a cluster is displaced one lattice site. The event is randomly chosen from all possible events, with each event weighted according to its probability. When a cluster moves into a site containing film, the film is moved into the wake of the cluster to preserve the number of film sites. Only those in contact with both a film and a vacuum site are permitted to move. The probabilities for void formation and/or dewetting and particle motion are given by $\beta\exp(-E_f/k_BT)$ and $\exp(-E_p/k_BT)$, respectively, where T is the temperature and k_B is the Boltzmann constant. The constant β sets the relative rates of dewetting and cluster motion. For void formation and dewetting, the barrier E_f is $\Delta H_{f\rightarrow v}$, which is the change in energy for conversion of the film site to a vacuum site. For the conversion of site F in Fig. 5(a), $\Delta H_{f\rightarrow v}=2\varepsilon_{ff}+1\varepsilon_{fp}$. For cluster motion, $E_p=\alpha\Delta H_{p\rightarrow v}+\Delta H_{\text{motion}}$, where $\Delta H_{p\rightarrow v}$ is for the conversion of all of the connected particle sites to vacuum sites and α is a constant $(0<\alpha\leq1)$. The barrier is adjusted by a capillary force given by ΔH_{motion}, which results from the motion of the entire particle and the displaced film sites. For the change from (a) to (b), $E_p=\alpha(3\varepsilon_{fp})+(3\varepsilon_{ff}-2\varepsilon_{fp}-1\varepsilon_{pp})$.

The simulation parameters were chosen to reflect the limited mobility of the clusters on the buffer; the simulation results were robust to changes in their values as long as cluster mobility was limited. In all simulations, $\varepsilon_{ff}=12k_BT$ (for reference, the cohesive energy of Xe is $32k_BT$ at 60 K). By assuming that particles were coated with a layer of Xe, ε_{fp} and ε_{pp} were set to $\frac{3}{2}\varepsilon_{ff}$, and α was set to 10%. The initial clusters occupied four sites and the lattice contained 512×512 sites, which corresponds to a region of about 2.5×2.5 μm in the Au-Xe system. Values for β ranged from 10^8 to 10^{24}. Increases in β resulted in decreased aggregation, as void nucleation and dewetting increased relative to particle motion. This range of values for β resulted in sizes and densities consistent with Au deposited on buffers ranging from 20 to 60 ML.

Figures 5(c) and 5(e) show the initial and final states of a simulation with a particle coverage of 10%. Figure 5(d), which is an intermediate configuration, can be qualitatively compared to the image in Fig. 3(a). The simulation gives an indication of the interaction of the clusters with the dewetting front as revealed by the shape of the front in Fig. 5(d). Without the addition of clusters to the simulation, the voids remain square as they grow. Experimental evidence for the suppression of dewetting can be found in the shapes of the fronts and the difference in the amount of dewetting in Figs. 2 and 3 (70% of the surface dewet at 64 K without clusters compared to 20% at 65 K with clusters). Unlike the case for liquid films, wherein pinning results in a flow toward the front,[26] pinning in solid films results in shedding of the clusters from the dewetting front in a manner similar to islands left behind as thin metal films dewet.[27] Islands of Xe are left behind as clusters inhibit the Xe surface diffusion. These islands are visible in Fig. 5(d) and are evidenced by the areas surrounding some of the particles in the dewet region of Fig. 3(b) that do not have small clusters in them.

The fact that particles irreversibly stick leads to shapes similar to those observed in DLCCA. Therefore, we compared experimental and simulated particle shapes by using the Hausdorf fractal dimension d as defined by $A\propto R^d$, where R is the average distance from the centroid to the perimeter

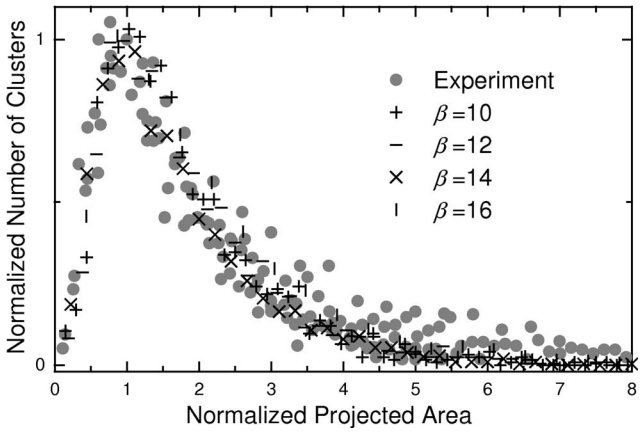

FIG. 6. Normalized size distribution for clusters formed by using the dewetting simulation and experimental data from Ref. 7 for six samples resulting from 5 Å Au depositions onto Ar, Kr, and Xe buffers ranging from 32 to 128 ML. The simulations involved three runs for each β, using values of 10^{10}, 10^{12}, 10^{14}, and 10^{16}. They resulted in ramified shapes with average sizes ranging from 47 to 19 lattice sites (individual cluster sizes were all multiples of 4). The sizes collapse into a single distribution after independent normalization of the data for each experiment or value of β.

of a cluster and A is its area. For 5 Å of Au deposited on Xe of different thicknesses, wherein coverages ranged from 9% to 21%, the measured fractal dimension was 1.72 ± 0.03.[24] Analysis of over 7000 clusters produced by the simulation that used 10% and 21% coverages yielded fractal dimensions of 1.70 and 1.76, respectively.

Figure 6 shows a comparison of the normalized size distributions of clusters produced by the simulation (10% coverage and various values of β) with those of clusters produced through experiments on Ar, Kr, and Xe buffers.[7] We conclude that the model provides good agreement with experimental cluster shapes, fractal dimensions, and size distributions.

This is a coarse-grained simulation and it has inherent limitations. The simulation is designed to provide and predict spatial and temporal structural arrangements, but not provide an atomistic view of the process. Neglected are atomic rearrangements of the clusters. Experimental observations indicate that the surface coverage remains constant for Au aggregates formed on Xe films greater than ~30 ML,[24] indicating that Au restructuring does not play a significant role for thicker films. Coalescence is important for the smaller particles produced on thinner films. The simulation also does not account for grain boundaries in the buffer. Indeed, voids nucleate at random locations. The simulation does produce particle shapes and distributions consistent with those of experimental particles both during and after buffer removal, as evidenced by the thermal cycling experiments.

E. Particle motion with the dewetting front

The simulations make it possible to follow particles during the aggregation process, tracking the distance each particle moves, something inaccessible during our experiments. Figure 7 plots this distance as a function of (a) the cluster coverage and (b) the thickness of the film. Film thicknesses were simulated by changing β in the simulation, and thicknesses were determined from the empirical relationship of $n \propto \theta^{-2.41}$, where n is the final number density of the clusters and θ is the thickness of the Xe film.[24] Figure 7(a) indicates that decreasing the amount of cluster material results in a power law increase in the distance that the particles move during aggregation. Figure 7(b) shows a linear increase in the distance with buffer thickness. This increased motion leads to increased aggregation, which accounts for the experimentally observed power law behavior of particle size and density with buffer thickness. These results indicate that the amount of material and buffer thickness can be used as control parameters for the spatial distribution of clusters.

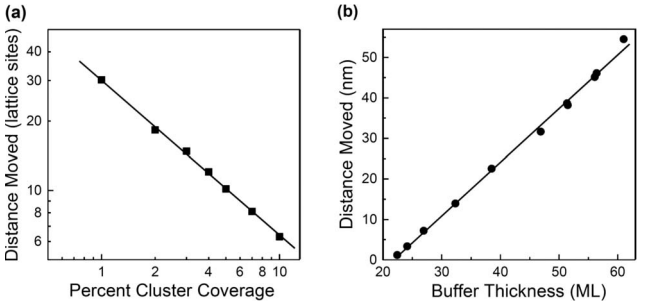

FIG. 7. Plots of the distance that particles move in the simulation as a function of (a) cluster coverage ρ and (b) buffer thickness θ. The fits indicate that the distance moved is proportional to the thickness of the buffer and $\rho^{-2/3}$. Buffer thickness and distances in (b) are determined by correlating sizes and number densities to experimental data for 5 Å of Au deposited on Xe buffer layers from Ref. 24.

Figure 8 demonstrates the experimental effect of cluster coverage and buffer thickness on cluster motion. The clusters in Fig. 8(a) result from a 1 Å Au deposition onto a 40 ML Xe buffer. There are some areas without clusters because they were removed by the dewetting front. These areas are even more evident in Fig. 8(b), wherein 1 Å of Au was deposited on a 100 ML Xe buffer. In this case, the particles form a network of lines that indicate where voids converged

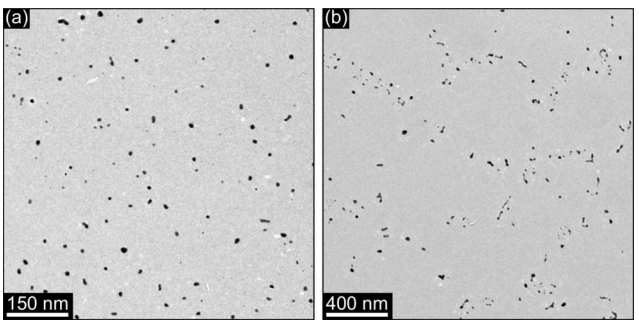

FIG. 8. Cluster movement with the dewetting fronts results in a higher concentration of them where dewetting fronts converge. Comparing the results of 1 Å of Au deposited on (a) 40 ML Xe and (b) 100 ML Xe indicates that particles move further on thicker films, resulting in a network of particles deposited where growing voids in the Xe film came together. On the thinner film, there are areas without clusters, but no clear network.

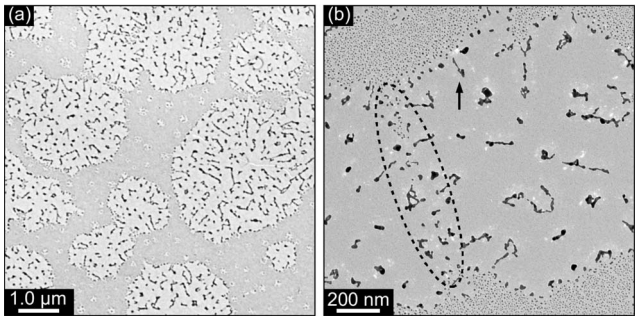

FIG. 9. The dewetting and aggregation processes were interrupted for 5 Å of Au deposited on a 100 ML Xe film by condensing a layer of amorphous ice over the partially dewet Xe film. The ice held the particles in place and prevented further dewetting as the Xe sublimed. (a) shows that many void areas had formed, as is evident by the presence of clusters. The smaller, high density clusters are not resolved in the low magnification image and result in a darker gray background, wherein particles remained on the Xe when the H_2O was condensed. The higher magnification image in (b) shows a region where two voids came together, resulting in a high density of large aggregated clusters.

as they spread in the Xe film. Assuming isotropic spreading of the dewetting front, voids formed in the center of the observed network and then spread out, sweeping the particles with the fronts. Eventually, the spreading voids collided and the clusters were deposited where the fronts came together. Comparing Fig. 8(b) to Figs. 1(b) and 8(a) demonstrates that this process is most dramatic for thick films and small cluster coverages, when clusters have a greater chance for motion.

This accumulation of particles at the dewetting front can be observed by using a capping layer of ice to stop the dewetting process. The results shown in Fig. 9 were obtained with a sample that was prepared by depositing 5 Å of Au onto a 100 ML film, heating, and then condensing a layer of amorphous ice over the partially dewet film. Figure 9(a) shows a low magnification image wherein the dewet regions are approximately round and contain ramified structures. Some of the voids have started to come together. Figure 9(b) presents a higher magnification image and the oval emphasizes a region where two voids met. Previous observations of networks of higher coverage areas like these were attributed to trapping of the clusters at grain boundaries.[15] Here, the observation of the formation of such networks makes it clear that they are formed by the motion of the particles with the dewetting front.

F. Effect of clusters on dewetting

The simulations discussed in Sec. III D suggest that the clusters strongly affect the shape of the dewet regions. By using the techniques applied to the samples in Figs. 2 and 3(b), we can follow the dewetting process by thermal cycling to different temperatures. The images in Fig. 10 were obtained after heating 40 ML Xe films to 59.8–66.3 K and then depositing Au at 20 K to mark the dewet regions. Again, the high-density darker gray regions indicate where the film had dewet. Figures 10(a) and 10(b) indicate how pure Xe films

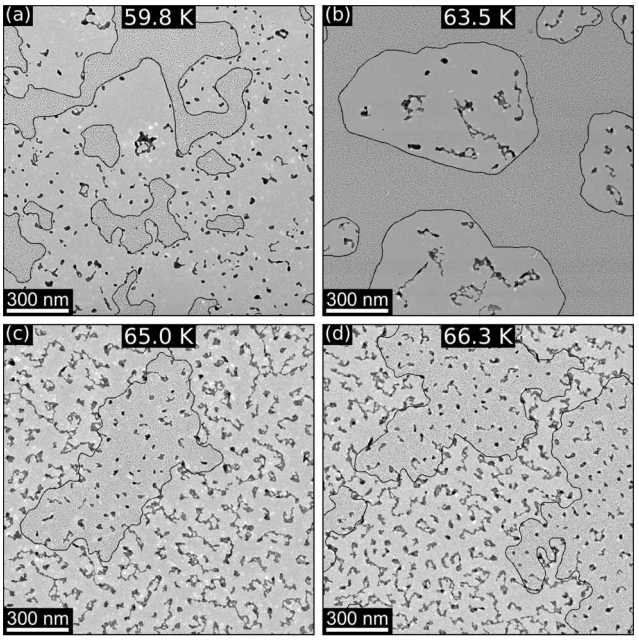

FIG. 10. Images showing the dewetting of 40 ML Xe films for a series of thermal treatment temperatures. In (a) and (b), no gold was deposited prior to warming, while in (c) and (d), 5 Å of Au was deposited prior to the heat treatment. Dewetting exposed 14%, 55%, 10%, and 66% of the *a*-C surface in (a)–(d). The dewet regions were determined by depositing 5 Å of Au at 20 K after temperature cycling, resulting in the formation of small, unresolved clusters. The dewet regions are evident from the darker gray regions, and the dewetting boundaries are highlighted by lines.

dewet, with Au deposited afterward. For Figs. 10(c) and 10(d), 5 Å of Au was deposited prior to the heat treatment and more Au was subsequently added. The lines in the images emphasize the locations and shapes of the dewet regions.

Figure 10 shows that the front is much smoother for the pure film [Figs. 10(a) and 10(b)] and that the voids become connected at a much earlier stage. In Fig. 10(a), Xe still covers 86% of the surface, yet several of the voids are connected. As dewetting continues, the film breaks up into islands, as in Fig. 10(b), wherein 45% of the surfaces is still covered. This suggests that the Xe microstructure plays an important role in dewetting of the pure films. Voids formed at grain boundary triple points can become connected as dewetting occurs fastest in the thinned grain boundaries. Thus, the dewetting would be fastest along the higher energy grain boundaries. The effect of the microstructure is also evident by the faceting apparent along the dewetting fronts of Fig. 10(a) and the islands in Fig. 10(b). For films with clusters [Figs. 10(c) and 10(d)], the effects of the microstructure are not visible, and the overall void shapes are more isotropic. This is even more evident for thicker films, as in Fig. 9. In contrast to the pure Xe films, the films with particles shown in Figs. 10(c) and 10(d), wherein 90% and 34% of the surface is covered, do not break up into islands and the voids remain isolated.

Another key feature apparent from Fig. 10 is that higher temperature heating cycles are required for the dewetting of

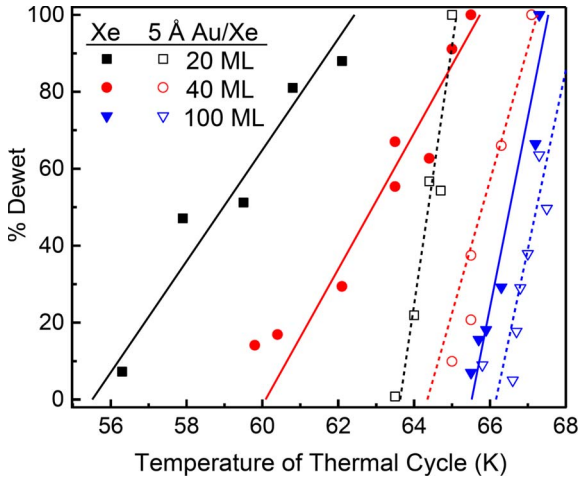

FIG. 11. (Color online) The amount of dewetting as a function of heating temperature for Xe films of 20, 40, and 100 ML initial thicknesses, with (open symbols) and without (closed symbols) Au particles. The amount of dewetting was determined as in Fig. 10. The lines are fits through the data.

films with clusters compared to pure Xe films. This effect can be quantified through Fig. 11, wherein the amount of dewetting is plotted as a function of thermal cycling temperature for films with and without 5 Å of Au. The plot makes it apparent that the clusters inhibit the dewetting process.

A comparison of different buffer thicknesses for pure films indicates the competition between dewetting and sublimation processes. Both the 20 and 40 ML films had finished dewetting and had sublimed by the time that the 100 ML film had started to dewet. This indicates that significant sublimative thinning occurs for the 100 ML film prior to dewetting; the amount, however, is unknown because the rate of sublimation is dependent on the morphology of the film. Figure 11 also indicates that the temperature range for dewetting overlaps with the range for sublimation. If dewetting occurred without any desorption, there would be a plateau region where the dewet film was stable instead of the continuous decrease in Xe coverage observed in Fig. 11. Because particle sizes formed by BLAG are strongly dependent on the thickness of the buffer, the more ramified structures in Fig. 10(b) compared to those in Fig. 10(a) suggest that the areas covered by Xe were thicker when the Au was deposited. This indicates that the film thickens in regions, even as sublimation is occurring.

Clusters on the film inhibit the dewetting process, such that it occurs at a higher temperature, resulting in more sublimation during the dewetting. The steeper slopes of the dotted lines (Au covered Xe) than the solid lines (pure Xe) in Fig. 11 and the lack of variation in cluster sizes between Figs. 10(c) and 10(d) also suggest that sublimation is more dominant and that less thickening occurs.

A key feature that can be deduced from Figs. 10 and 11 is that the void nucleation and the dewetting processes are controlled by Xe diffusion and that the clusters inhibit those processes. Figure 11 shows that the clusters delay the nucleation of voids and thus act to stabilize the film. These results are similar to those of adding a second slower moving species to a thin metal film.[28] In that case, the slower diffusing species accumulate at the edge of a grain and slow grain boundary grooving. Here, the clusters are much slower moving than Xe atoms and they inhibit the nucleation of voids. Clusters at the dewetting front further inhibit Xe diffusion and slow the movement of the front. As a result, the temperature where void nucleation and dewetting occur increases for decorated films.

The Xe desorption temperature is raised by the particles, as shown in Fig. 11 by the complete desorption of the pure 20 ML film before the onset of dewetting for the 20 ML film with Au. 5 Å of Au deposited onto a thin buffer results in ~20% of the *a*-C surface being covered with Au after warming to room temperature. The Au coverage on Xe will even be higher at low temperature with less cluster coalescence. The high Au coverage and the stronger Au-Xe binding energy [0.214 eV compared to the Xe cohesive energy of 0.167 eV (Ref. 29)] significantly impede Xe sublimation. This is supported by the simulation, which indicates that the time required for the removal of the buffer increased fourfold as the cluster coverage increased from 1% to 10%. Without this higher desorption temperature, significant sublimation would occur prior to dewetting and less aggregation would occur.

G. Xe island coarsening

Figure 10(b) shows that there were islands of Xe that had sizes larger than the features in Fig. 10(a), which suggests that Xe was moving on the *a*-C substrate and that the islands were coarsening. To quantify the changes in size, we define a correlation function, which is given by the probability that two points separated by a distance x will both be in a region with Xe or both in a dewet region. For $x=0$, the probability is 1, and for $x \gg 0$, the value is determined by the average Xe coverage of the surface. The correlation length is defined as the distance required for the correlation function to drop by a value of $1/e$.[30]

Figure 12 plots the correlation lengths as a function of the amount of dewetting for pure Xe films and for Xe films with Au particles. For pure Xe, the correlation length increases with the amount of dewetting. Even during sublimation, large islands continue to grow. This indicates an Ostwald ripening process where smaller islands lose atoms to larger islands by diffusion of Xe over the *a*-C surface. This accounts for the large island sizes in Fig. 10(b). Another notable feature of Fig. 12(a) is that the correlation lengths are not dependent on film thickness.

The correlation lengths for dewetting films with clusters are shown in Fig. 12(b). As in Fig. 12(a), the correlation length initially increases with dewetting, but then levels off and starts to drop. This occurs as voids in the Xe grow and begin to converge, and the remaining Xe regions shrink through sublimation. With the presence of clusters on the film, sublimation dominates over any ripening. The 20 ML film in Fig. 12(b) has significantly lower correlation lengths than the thicker films. Images of these thin films indicate that they break up, as for the pure films, but that there is no significant restructuring to form faceted islands. For thicker

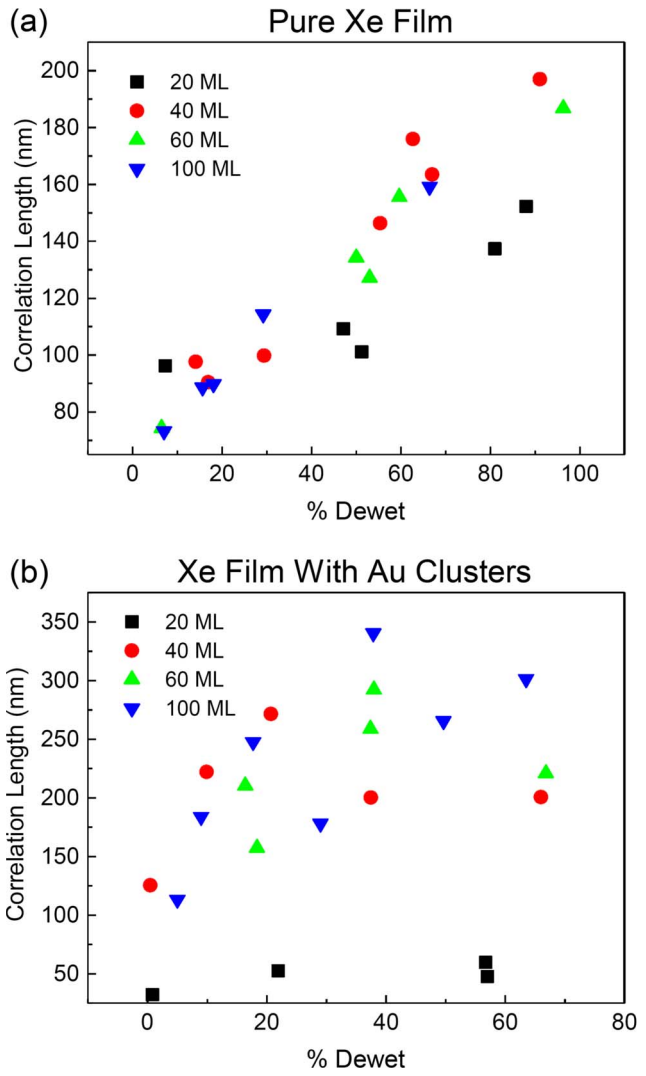

FIG. 12. (Color online) Plots of the correlation lengths for partially dewet Xe films having initial thicknesses of 20, 40, 60, and 100 ML. A comparison between dewetting of (a) pure Xe films and (b) Xe films decorated with Au particles shows that the particles inhibit void nucleation and island coarsening.

films, the maximum correlation length for each thickness increases with thickness, but the considerable spread in the data dominates the trend with film thickness.

The correlation length during the early stages of dewetting provides some indication of the density of voids that form in the film. Direct counting shows that the densities of voids were similar for 20, 40, 60, and 100 ML pure films and 20 ML films with clusters ($\sim 3 \times 10^8$ voids/cm^2). The density of voids was significantly lower ($\sim 5 \times 10^7$ voids/cm^2) for 40, 60, and 100 ML films with clusters. The networks of polygons such as those in Fig. 8(b) provide another way to determine the void density. While the density of polygons is related, it is not a direct measure of the density of the initial voids.[31] Some voids that have met in Fig. 9(a) suggest that when voids that are small compared to the final polygon size come into contact, material can be drained from the contact, allowing the voids to merge. Previously, it was observed that the density of the polygons has a weak exponential dependence on the buffer condensation temperature,[15] which suggests that changes in buffer condensation conditions result in differences in the initial void density.

The changes in correlation length and void densities provide insight into the mechanism of void nucleation. The similar void densities on the pure films and the 20 ML films with clusters suggest that defects lead to void nucleation. The temperature dependence of the void density[15] indicates that the number of voids decreases with increasing film deposition temperature. This suggests that defects in the Xe film rather than on the substrate influence void nucleation. Voids will be more likely to nucleate at the defects or at high energy grain boundaries. Therefore, the density of voids is related more to the defects than the grain size. Growth at higher temperature results in both larger grains and fewer defects in the film, leading to the nucleation of fewer voids during dewetting.

In the absence of clusters, Xe diffusion readily leads to void nucleation at the defects. For the 20 ML films with clusters, Xe diffusion is impeded, but the thin film still provides easy void nucleation. For thicker films with clusters, void nucleation is impeded and becomes the slower process. Once formed, void growth dominates over the nucleation of new voids. This results in a much lower void density and a larger correlation length as the voids grow without impinging. Films with a high density of initial voids have more voids converging, which results in much smaller features. Larger structures are formed only through Ostwald ripening and restructuring.

H. Comparison with other dewetting systems

Insight into the cluster aggregation process can be gleaned from other dewetting systems. As mentioned above, Xe islands containing Au clusters are left behind the dewetting front in a manner similar to thin metal film agglomeration. Parallels also occur in the dewetting and breakup of thin polystyrene films that were annealed above their glass transition temperature.[31] For polymer films, void formation results from thermal fluctuations in the liquid, while void nucleation in our crystalline film results from grooving at grain boundaries and/or defects. In both cases, void expansion is driven by surface energies.

As voids in the polymer film expand, material accumulates at the dewetting front. This results in the formation of networks of particles similar to those in Fig. 8(b). Built up material can be left behind such that not all of the material is carried to where the voids meet, as with Xe films decorated with Au. This material forms fingers along the front, which break off as the front moves, leaving behind droplets as in the agglomeration of thin metal films during annealing.[27] We envision that a similar process occurs with Xe films. The observation of clusters that jut out perpendicular to the dewetting front, as highlighted by the arrow in Fig. 9(b), supports this assumption.

BLAG results in cluster sizes and densities that have a power law dependence on the thickness of the buffer layer. Similarly, the sizes and densities of droplets formed by dewetting of the polymer films result in a power law dependence

on the thickness of the polymer film. For polymers, the parameters for the power law relationship are dependent on the substrate. For BLAG, the substrate dependence has not been investigated, but the cluster material does play an important role in those parameters.[7]

The shapes of the structures produced by BLAG and from polymer films are very different. Polymer films in the liquid state produce spherical droplets. In BLAG, the aggregation of metal particles occurs at low temperature and Au coalescence is very limited. As a result, compact structures are observed only for small particles, and ramified shapes are produced with larger particles or more extended aggregates..

The assembly of nanoparticles during dewetting and desorption of liquid films is also analogous to BLAG. Again, particles move with the dewetting front during void nucleation and spreading in liquid films.[32] In contrast to liquids, however, particle motion is limited to the front and diffusion in the bulk of the film is insignificant. The particle-particle interactions in liquid films are also altered by the presence of capping agents, which alters the shapes of the aggregates.

IV. CONCLUSIONS

We have introduced a different model for the aggregation of clusters during BLAG, wherein particle motion is driven by capillary forces during dewetting and sublimation of the buffer. Particles aggregate along the dewetting front, and the distance they move is determined by the thickness of the buffer and the density of the particles. The particles inhibit Xe diffusion and significantly alter the dewetting and sublimation processes. This dewetting-driven model suggests that the microstructures of the substrate and the film play a role in the BLAG process. For example, steps on a surface may act as nucleation sites for dewetting, leading to cluster decoration of steps, as observed on the Pt(997) surface.[33] Differences in wetting characteristics may account for the formation of compact structures on some substrates, even with thicker buffers.[34] Regardless of the substrate, significant diffusion of Xe occurs prior to desorption, indicating that data previously interpreted as suggesting layer-by-layer desorption should be reevaluated to account for dewetting.[35]

ACKNOWLEDGMENTS

Early stages of this work were supported in part by the U.S. Department of Energy, Division of Materials Sciences under Grant No. DEFG02-01ER45944. The TEM imaging was carried out in the Frederick Seitz Materials Research Laboratory Central Facilities, University of Illinois, which are partially supported by the U.S. Department of Energy under Grants No. DE-FG02-07ER46453 and No. DE-FG02-07ER46471. The authors thank C. M. Aldao for valuable feedback on the simulation.

*Present address: Department of Physics, COMSATS Institute of Information Technology, Jauhar Campus, Islamabad, Pakistan.

[1] P. A. Kralchevsky and K. Nagayama, Adv. Colloid Interface Sci. **85**, 145 (2000).
[2] M. Maillard, L. Motte, A. T. Ngo, and M. P. Pileni, J. Phys. Chem. B **104**, 11871 (2000).
[3] R. D. Deegan, O. Bakajin, T. F. Dupont, G. Huber, S. R. Nagel, and T. A. Witten, Nature (London) **389**, 827 (1997).
[4] R. D. Deegan, O. Bakajin, T. F. Dupont, G. Huber, S. R. Nagel, and T. A. Witten, Phys. Rev. E **62**, 756 (2000).
[5] J. H. Weaver and G. D. Waddill, Science **251**, 1444 (1991).
[6] L. Huang, S. J. Chey, and J. H. Weaver, Phys. Rev. Lett. **80**, 4095 (1998).
[7] V. N. Antonov, J. S. Palmer, A. S. Bhatti, and J. H. Weaver, Phys. Rev. B **68**, 205418 (2003).
[8] V. N. Antonov, J. S. Palmer, P. S. Waggoner, A. S. Bhatti, and J. H. Weaver, Phys. Rev. B **70**, 045406 (2004).
[9] J. Krim, J. G. Dash, and J. Suzanne, Phys. Rev. Lett. **52**, 640 (1984).
[10] M. A. Torija, A. P. Li, X. C. Guan, E. W. Plummer, and J. Shen, Phys. Rev. Lett. **95**, 257203 (2005).
[11] P. Swaminathan, V. N. Antonov, J. A. N. T. Soares, J. S. Palmer, and J. H. Weaver, Phys. Rev. B **73**, 125430 (2006).
[12] P. S. Waggoner, J. S. Palmer, V. N. Antonov, and J. H. Weaver, Surf. Sci. **596**, 12 (2005).
[13] E. Gross, Y. Horowitz, and M. Asscher, Langmuir **21**, 8892 (2005).
[14] T. Irawan, D. Boecker, F. Ghaleh, C. Yin, B. V. Issendorff, and H. Hövel, Appl. Phys. A: Mater. Sci. Process. **82**, 81 (2006).
[15] J. S. Palmer, V. N. Antonov, A. S. Bhatti, P. Swaminathan, P. S. Waggoner, and J. H. Weaver, Surf. Sci. **595**, 64 (2005).
[16] C. M. Kennefick and R. Raj, Acta Metall. **37**, 2947 (1989).
[17] D. C. Agrawal and R. Raj, Acta Metall. **37**, 2035 (1989).
[18] Kr can be capped with Xe, as was previously done without thermal cycling (Ref. 7), and the results are similar, but the lower desorption temperature makes controlled thermal cycling more difficult.
[19] A. R. Miedema and B. E. Nieuwenhuys, Surf. Sci. **104**, 491 (1981).
[20] C. G. Zimmermann, K. Nordlund, M. Yeadon, J. M. Gibson, R. S. Averback, U. Herr, and K. Samwer, Phys. Rev. B **64**, 085419 (2001).
[21] I. G. Marchenko and I. M. Neklyudov, Low Temp. Phys. **32**, 957 (2006).
[22] T. R. Ohno, J. C. Patrin, U. S. Ayyala, and J. H. Weaver, Phys. Rev. B **44**, 1891 (1991).
[23] C. G. Zimmermann, M. Yeadon, K. Nordlund, J. M. Gibson, R. S. Averback, U. Herr, and K. Samwer, Phys. Rev. Lett. **83**, 1163 (1999).
[24] C. Haley and J. H. Weaver, Surf. Sci. **518**, 243 (2002).
[25] E. Rabani, D. R. Reichman, P. L. Geissler, and L. E. Brus, Nature (London) **426**, 271 (2003).
[26] R. D. Deegan, Phys. Rev. E **61**, 475 (2000).
[27] E. Jiran and C. V. Thompson, J. Electron. Mater. **19**, 1153 (1990).
[28] M. Bouville, D. Chi, and D. J. Srolovitz, Phys. Rev. Lett. **98**,

085503 (2007).
[29] G. Vidali, G. Ihm, H. Y. Kim, and M. W. Cole, Surf. Sci. Rep. **12**, 135 (1991).
[30] The correlation length l is determined by fitting to the function $f(x)=[f(0)-f(\infty)]\exp(-x/l)+f(\infty)$, where $f(0)=1$, $f(\infty)=(\rho)^2(1-\rho)^2$, and ρ is the fraction of the substrate covered by Xe. The data were fitted over the first two correlation lengths. Over this length scale, the data exhibited exponential decay.
[31] G. Reiter, Langmuir **9**, 1344 (1993).
[32] P. C. Ohara and W. M. Gelbart, Langmuir **14**, 3418 (1998).
[33] J. Zhang, D. Repetto, V. Sessi, J. Honolka, A. Enders, and K. Kern, Eur. Phys. J. D **45**, 515 (2007).
[34] G. Kerner, Y. Horowitz, and M. Asscher, J. Phys. Chem. B **109**, 4545 (2005).
[35] G. Kerner, O. Stein, Y. Lilach, and M. Asscher, Phys. Rev. B **71**, 205414 (2005).